Effect of Filling Ratio on the Entrainment Limit of Large-Scale Heat Pipe with 3D-Printed Wick Structure

Faruk Celik, Dong Hun Lee, Ye Yeong Park, In Cheol Bang*
Department of Nuclear Engineering, Ulsan National Institute of Science and Technology (UNIST)
50 UNIST-gill, Ulju-gun, Ulsan, 44919, Republic of Korea
** Corresponding author: icbang@unist.ac.kr*

***Keywords:** Heat Pipes, Entrainment Limit, Filling Ratio, Combined Wick

1. Introduction

Heat pipes are highly efficient devices that transfer large amounts of heat with minimal temperature difference, using phase change and capillary action. They are widely used in electronics cooling, aerospace, nuclear reactors, and renewable energy systems for their superior thermal performance and reliability. In nuclear reactors, heat pipes are key components in passive cooling systems, ensuring safe operation without external power. Notable examples include the eVinci microreactor [1], Aurora reactor [2], and the Kilopower Reactor Using Stirling Technology (KRUSTY) [3], all of which utilize heat pipes to enhance safety and efficiency.

Heat pipe performance is affected by factors such as working fluid, wick structure, inclination angle, aspect ratio, and filling ratio. Research has shown that these factors play a crucial role in determining efficiency and entrainment limits. For instance, Tian et al. [4] found that a 30° inclination angle optimizes thermal performance in potassium heat pipes. Seo and Lee [5] demonstrated that the aspect ratio influences the entrainment limit in water heat pipes. Sukchana and Jaiboonma [6] highlighted the significant impact of filling ratio on the thermal efficiency of R-134a heat pipes, while Lee and Bang [7] noted that high filling ratios in sodium heat pipes can cause liquid pooling at the condenser end, affecting heat transfer.

Previous studies have provided a foundation for understanding the effects of factors on short heat pipe performance, but how these factors interact with modern wick structures is still under-explored. The effect of the filling ratio on the entrainment limit is particularly critical. In this study, we examine how the filling ratio influences the entrainment limit in a 4-meter-long heat pipe with a 3D-printed combined wick structure, comparing experimental results with existing empirical correlations to assess their accuracy for advanced wick designs.

2. Entrainment Limit

In a working heat pipe, liquid and vapor move in opposite directions, creating a countercurrent flow. This flow is influenced by shear forces at the surface where the liquid and vapor meet, which can make it harder for the liquid to return to the evaporator. When this becomes significant, the heat pipe reaches its flooding limit [8]. Adding more heat increases vapor speed and wave action, making the liquid flow unstable. At this point, the shear forces at the interface may become strong enough to break the liquid's surface tension, causing liquid droplets into the vapor and carried to the condenser section. This occurrence is shown in Fig. 1.

Previous studies have proposed many models to describe the shear-induced entrainment limitation. In an initial effort to forecast the entrainment limit in functional heat pipes, Cotter [9] utilized the concept of hydrodynamic instability on horizontally wicked heat pipes. He derived an equation for the critical wavelength based on the air/vapor velocity. The correlation for the entrainment limitation is determined by the velocity-based energy balance. Kemme [10] developed a model to forecast the entrainment limit for gravity-assisted sodium heat pipes equipped with screen wicks.

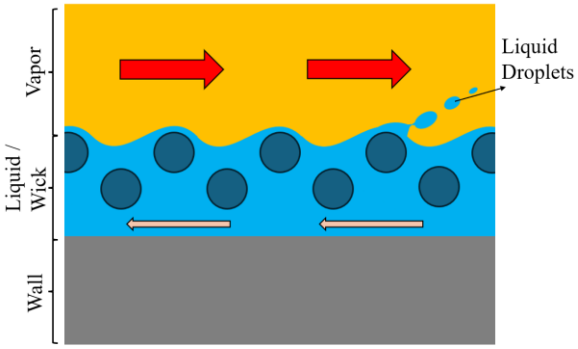

Fig. 1. Illustration of shear-induced entrainment.

This model incorporated a buoyancy force term into the entrainment equation initially formulated by Cotter. Chi [11] introduced a technique for estimating the entrainment limit in capillary-wicked heat pipes by utilizing a force balance approach. Prenger [12] formulated a correlation for gravity-assisted heat pipes. The model incorporated both liquid and vapor inertia terms. However, it was discovered that the liquid inertia term was dominant because the liquid was somewhat shielded from the vapor flow. Therefore, the vapor inertia term was neglected in the correlation. Tien and Chung [13] presented an entrainment limit correlation by using the Kutateladze flooding criterion for the horizontal, vertical, grooved heat pipes. The other entrainment limit approach is introduced by Rice and Fulford [14]. They hypothesized that the sole pressure difference between the liquid in the mesh and the vapor

is the kinetic head of the flow. The mentioned correlation is listed in Table I.

In the context of most correlations, the parameter L typically represents the characteristic length associated with the capillary wick structure [8]. This characteristic length is a critical factor that influences the capillary pressure and, consequently, the overall efficiency of liquid transport within the system. In this study, L is specifically defined as the effective pore diameter of the wick structure. In the Kemme model, Ω defines the dimensionless flow factor which varies from 1.1 to 1.234 for laminar regime and is 2.2 for turbulent flow regime [8,15]. In the calculations, it is assumed as the turbulent flow. Furthermore, the parameter C_k is a constant introduced by Kutateladze, which is adopted as a value of $\sqrt{3.2}$ [5]. The thermophysical properties of water, particularly those relevant to the system's operating conditions, were obtained from the National Institute of Standards and Technology (NIST) database [16]. These properties were selected based on saturation conditions.

Table I: Empirical correlations for entrainment limitation of gravity-assisted heat pipe.

Researcher	Entrainment Limitation (Q_e)
Cotter (1967)	$A_v h_{fg}\left(\frac{2\pi\rho_v\sigma}{L}\right)^{1/2}$
Kemme (1976)	$A_v h_{fg}\left[\left(\frac{\rho_v}{\Omega}\right)\left(\frac{2\pi\sigma}{L}+\rho_v g D_h\right)\right]^{1/2}$
Chi (1976)	$A_v h_{fg}\left(\frac{\rho_v\sigma}{L}\right)^{1/2}$
Prenger (1984)	$2A_v h_{fg}\frac{D_{wire}}{D_{pipe}}\left(\frac{\rho_l\sigma}{\pi D_{pipe}}\right)^{1/2}$
Tien and Chung (1979)	$C_k^2 A_v h_{fg}\left(\frac{\sigma}{L}\right)^{0.5}\left(\rho_l^{-1/4}+\rho_v^{-1/4}\right)^{-2}$
Rice and Fulford (1987)	$A_v h_{fg}\left(\frac{8\rho_v\sigma}{L}\right)^{1/2}$

The plot illustrates the differences between the predictions of maximum heat transfer capacity by the various models arise primarily from the distinct assumptions and methodologies used in each model to account for critical heat transfer mechanisms.

3. Experiment

3.1. Experimental setup

The large-scale water heat pipe test facility is designed to study the performance of a heat pipe system under various conditions. The experimental setup uses a 4-meter-long heat pipe with a 3D-printed wick structure, with inner and outer diameters of 22 mm and 25.4 mm. The porosity of wick structure is 0.44. The inner and outer diameters of wick structure are 14mm and 20 mm respectively. The 2-meter evaporator section uses furnace heaters for consistent heating, while a vacuum pump maintains the necessary low-pressure environment. The 1-meter condenser section is equipped with a cooling jacket for heat removal. Internal pressure is monitored by two 4-20mA pressure transmitters, and temperature is measured by twenty K-type thermocouples spaced 20 cm apart, along with additional thermocouples at the cooling jacket inlet and outlet. A turbine-type flow meter measures coolant flow rate. To assess heat loss, eight thermocouples are placed on the outer surface of the insulation. Figure 3 illustrates the system setup. Initially, the heat pipe is filled with the working fluid according to a predetermined filling ratio, calculated as the ratio of fluid volume to evaporator volume. The vacuum pump establishes the desired internal pressure. For each filling ratio, the heat pipe is drained, dried, and refilled, then the heat is gradually increased until the entrainment limit is reached while controlling heat removal with coolant flow.

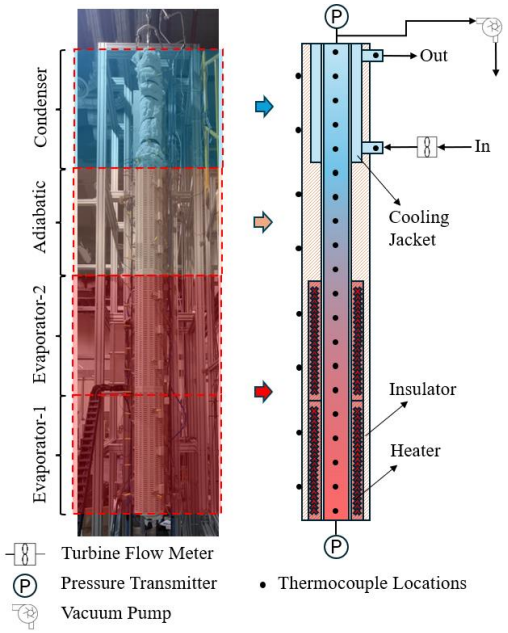

Fig. 3. Demonstration for experimental system.

The maximum allowable transport power before the onset of entrainment is determined by the rejected power by the cooling jacket at the point where fluctuations in the wall temperature begin to occur.

3.2. Characteristics of 3D-printed combined wick structure

To efficiently transfer heat over long distances through the wick structure with minimal fluid resistance, high capillary force and permeability should be achieved. This study used combined lattice wick structures. The wick features two types of lattices: a diamond lattice for the inner layer to enhance driving force and heat transfer, and two cubic lattice layers for the outer layer to improve

permeability [17]. The combined lattice wick structure was fabricated using metal 3D-printing. This method overcomes traditional manufacturing limits and improves thermal performance by enhancing surface roughness. The stainless steel 316L powder was used for wick fabrication.

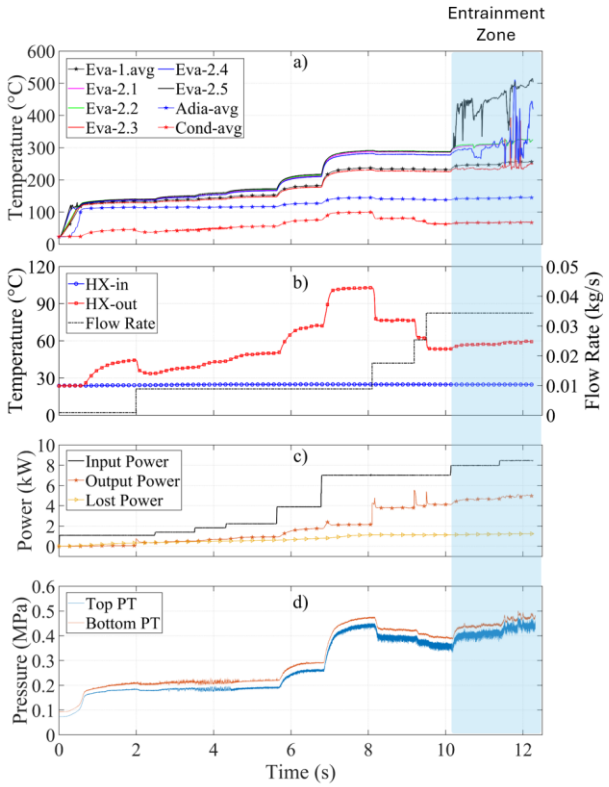

Fig. 4. Transient variations in a) wall temperature, b) coolant temperature and flow rate, c) input, output, and lost power, and d) internal pressures, at 100% filling ratio with an initial pressure of 75 kPa.

4. Results and Discussion

The experimental results for each filling ratio and internal pressure were analyzed to understand when entrainment begins. All measurements obtained from the experimental setup are comprehensively displayed in Figure 4, focusing on the system's behavior at a 100% filling ratio and an initial internal pressure of 75 kPa. As the input power increased, both temperature profiles and internal pressure rose systematically. The wall temperature profiles stabilized under allowable power, indicating steady thermal performance. However, as power approached the system's limit, temperature profiles began fluctuating, signaling instability near critical conditions like the entrainment limit. Further power increases led to erratic temperature behavior and extreme instability, culminating in a dry-out condition, where inadequate liquid cooling caused a sharp temperature rise. During entrainment onset, an audible sound of liquid droplets was also observed, similar to findings in Kemme's research [18]. The analysis shows that most models overestimate the maximum heat transfer capacity (Q_{max}) compared to the experiments, especially at lower filling ratios as shown in Figure 5.

Chi's model aligns well with experimental data at 100% and 80% filling ratios, suggesting it better accounts for systems with higher fluid content. Conversely, Prenger's model provides a better prediction at the 60% filling ratio, indicating its potential suitability for lower fluid conditions where the system's performance is more constrained.

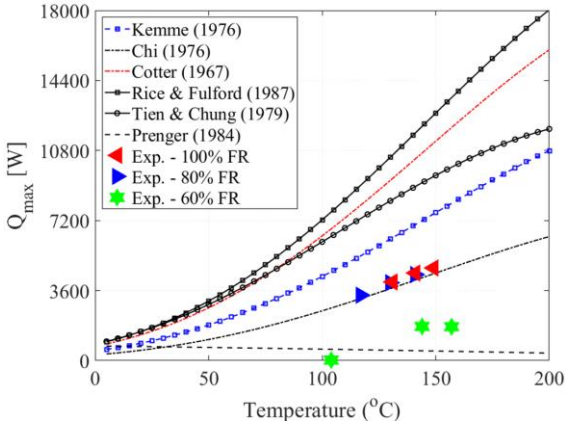

Fig. 5. Comparison between entrainment limit correlations.

These discrepancies between the models and experimental data suggest that the theoretical models may not fully capture the complexities and inefficiencies that arise in real-world systems. Additionally, while all datasets—both experimental and theoretical—show an expected increase in Q_{max} with rising temperature, the rate of this increase varies. Some models predict a much sharper rise in Q_{max} than what is observed experimentally, where the increase is more gradual.

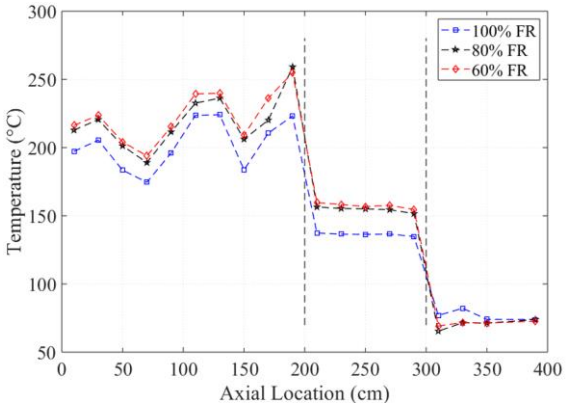

Fig. 6. Steady-state temperature profiles at 3970 W and 0.55 lpm coolant flow rate.

The steady-state temperature profiles along the axial length of the heat pipe are illustrated in Figure 6. Despite the variations in filling ratio, the temperature profiles exhibit similar overall trends. Among the three filling ratios, the 60% filling ratio displays the highest

temperature profile, particularly in the first half of the system. This elevated temperature indicates that the reduced liquid content in the system leads to less effective cooling, resulting in higher operating temperatures.

5. Conclusion

This study examined how the filling ratio affects the entrainment limit in a large-scale heat pipe with a 3D-printed wick structure. Results show that higher filling ratios improve thermal performance and delay entrainment, while lower ratios lead to greater temperature fluctuations and earlier instability. Comparing experimental data with theoretical models revealed that Chi's model predicts better at higher filling ratios, while Prenger's model is more accurate for lower ratios. The findings show the need to improve theoretical models to better account for various operating conditions.

ACKNOWLEDGMENT

This work was partly supported by the National Research Foundation of Korea (NRF) grant funded by the Korea Government (MSIT) (no. 2021M2D2A1A03048950) and Korea Institute of Energy Technology Evaluation and Planning (KETEP) grant funded by the Korea Government (MOTIE) (no. RS-2024-00403194, Next-Generation Nuclear Technology Creation IP-R&D Talent [Human Resources] Development Project).

REFERENCES

[1] A. Levinsky, J. J. van Wyk, Y. Arafat, M. C. Smith, "Westinghouse eVinci™ Reactor for Off-Grid Markets," *Transactions of the American Nuclear Society*, Vol. 119, Orlando, Florida, November 11–15, 2018.
[2] Oklo Inc. "Part II: Final Safety Analysis Report." *Aurora Safety Case*, Rev. 0, 2020.
[3] P. R. McClure, D. I. Poston, M. A. Gibson, L. S. Mason, R. C. Robinson, "Kilopower Project: The KRUSTY Fission Power Experiment and Potential Missions," *Nuclear Technology*, Vol. 206, pp. S1-S12, 2020.
[4] Z. Tian, X. Liu, C. Wang, D. Zhang, W. Tian, S. Qiu, G.H. Su, "Experimental Investigation on the Heat Transfer Performance of High-Temperature Potassium Heat Pipe for Nuclear Reactor," *Nuclear Engineering and Design*, Vol. 378, pp. 111182, 2021.
[5] J. Seo, J.-Y. Lee, "Length Effect on Entrainment Limitation of Vertical Wickless Heat Pipe," *International Journal of Heat and Mass Transfer*, Vol. 101, pp. 373–378, 2016.
[6] T. Sukchana, C. Jaiboonma, "Effect of Filling Ratios and Adiabatic Length on Thermal Efficiency of Long Heat Pipe Filled with R-134a," *Energy Procedia*, Vol. 34, pp. 298–306, 2013.
[7] D. H. Lee, I. C. Bang, "Experimental Investigation of Thermal Behavior of Overfilled Sodium Heat Pipe," *International Journal of Heat and Mass Transfer*, Vol. 215, pp. 124449, 2023.
[8] G. P. Peterson, B. K. Bage, "Entrainment Limitations in Thermosyphons and Heat Pipes," *Journal of Energy Resources Technology*, Vol. 113, September 1991.
[9] T. P. Cotter, "Heat Pipe Startup Dynamics," *Proceedings of the SAE Thermionic Conversion Specialist Conference*, Palo Alto, California, October, pp. 344-347, 1967.
[10] J. E. Kemme, "Vapor Flow Consideration in Conventional and Gravity Assisted Heat Pipes," *Proceedings of the 2nd International Heat Pipe Conference*, Bologna, Italy, March, pp. 11-21, 1976.
[11] S. W. Chi, "Heat Pipe Theory and Practice," Hemisphere Publishing Co., Washington, D. C., pp. 33-95, 1976.
[12] F. C. Prenger, "Performance Limits of Gravity-Assist Heat Pipes," *Proceedings of the 5th International Heat Pipe Conference*, pp. 1-5, 1984.
[13] C. L. Tien, K. S. Chung, "Entrainment Limits in Heat Pipes," *AIAA Journal*, Vol. 17, No. 6, p. 643, 1979.
[14] G. Rice, D. Fulford, "Influence of a Fine Mesh Screen on Entrainment in Heat Pipes," *Proceedings of The 6th International Heat Pipe Conference*, Grenoble, France, May, pp. 168-172, 1987.
[15] B.H. Kim, C.J. Kim, "Entrainment in Thermosyphons and Heat Pipes."
[16] National Institute of Standards and Technology (NIST), "Chemistry WebBook."Available at: https://webbook.nist.gov/
[17] Y. Y. Park, I. C. Bang, "Performance Analysis of Water Heat Pipe for Application of the Passive Cooling System in Nuclear Power Plants," *Nuclear Technology*, DOI: 10.1080/00295450.2024.2372509, 2024.
[18] J. E. Kemme, "High Performance Heat Pipes (Wicks Covered with Fine Screen for Capillary Action in High Performance Heat Pipes)," 1967.

NOMENCLATURE

A_v	vapor cross-sectional area (m^2)
h_{fg}	latent heat of vaporization (J/kg)
ρ_v	vapor density (kg/m^3)
ρ_l	liquid density (kg/m^3)
σ	liquid surface tension (N/m)
L	characteristic length of wick structure (m)
Ω	dimensionless flow factor
g	gravitational acceleration (m/s^2)
D_h	hydraulic diameter (m)
D_{wire}	wire diameter (m)
D_{pipe}	pipe inner diameter (m)
C_k	constant parameter of Kutateladze